IEEE Robotics and Automation Letters (RA-L) paper, presented at ICRA 2026, Vienna, Austria. Cite as RA-L paper.

A Dual-Adhesion-Enhanced Soft Gripper With Microwedge Adhesives and SMA-Driven Microspines

Chang Wang, Peijin Zi, Yang Luo, Bochao Song, *Graduate Student Member, IEEE*, Tao Zhang, *Member, IEEE*, Kun Xu, *Member, IEEE*, and Xilun Ding

***Abstract*—Soft grippers are highly valued for their adaptability and safety, but their inherent softness often leads to grasping failure under heavy loads. Most adhesion-enhanced grippers rely on single-adhesion strategies tailored for either smooth or rough surfaces. Lizards, however, effectively navigate in unstructured environments by seamlessly transitioning between different adhesion mechanisms based on surface conditions. Inspired by the hybrid adhesion strategies of geckos and chameleons, this study presents a bioinspired soft gripper that integrates microwedge dry adhesives and SMA-driven microspines. The microwedge adhesives provide controllable adhesion for smooth surfaces, while the SMA-driven microspines extend for rough-surface adhesion and retract to avoid interference. An optimization model was developed to determine optimal link dimensions, enhancing grasping performance in terms of force and radius. Experimental results on various surfaces validated its efficacy. Notably, the gripper with non-backed adhesives achieved 34.9 N payload and 260 mm grasping diameter, marking improvements of 209% and 117%, respectively, over the version without adhesives. In microspine mode, the gripper supported a 20.4 N payload and a 280 mm diameter. In tip clamping mode, the maximum payload reached 6.2 N when grasping a 2 cm block.**

***Index Terms*—Grippers and other end-effectors, soft robot materials and design, soft gripper, microwedge adhesive, microspine.**

I. Introduction

SOFT grippers, composed of flexible structures or materials, offer exceptional adaptability to targets with diverse shapes. In recent years, they have garnered significant attention due to their superior adaptability and safety compared with traditional rigid grippers [1], [2]. Based on actuator integration, soft grippers can be classified into embedded and non-embedded actuation types. Embedded actuation methods, including pneumatic-driven [3], [4], tendon-driven [5], [6], and smart material-driven systems [7], are commonly used. The additional air supply and high-pressure drive requirements limit the applicability of pneumatic and smart materials. Furthermore, these embedded actuation methods often compromise grasping adaptability. Non-embedded actuation grippers recently attracted growing interest [8], [9]. The bioinspired Fin Ray structure, known for passive adaption and non-embedded actuation, has become a research focus. This structure enables better surface conformity by wrapping around the force application point. Despite advancements in soft grippers, significant challenges remain, particularly their inherent softness, which can lead to grasping failure under high payloads.

To enhance grasping strength, researchers have investigated various methods such as interlocking fingers [10], soft-rigid coupling or variable stiffness mechanisms [11], [12], and adhesion technologies integration. Mechanical interlocking requires specialized fingertip interfaces to fully enclose the object, which limits the range of graspable objects. Soft-rigid coupling involves integrating rigid components into the soft fingers, with variable stiffness mechanisms allowing the adjustment of gripper stiffness. Both methods improve grasping strength by introducing rigid elements, but can compromise adaptability to various surfaces. In contrast, integrating adhesion technologies provides an effective solution that enhances grasping performance without sacrificing adaptability or reducing the range of graspable objects.

Existing grippers primarily integrate adhesion technologies, including electrostatic adhesion, vacuum suction, microspine adhesion, and dry adhesion [13], [14], significantly improving grasping force [15]. For instance, Chen developed the FinEA gripper with electroadhesion pads, achieving a 65% increase in shear load capacity under 4 kV. However, electrostatic adhesion requires high voltage, limiting its application environments. Fang et al. proposed an octopus-inspired vacuum sucker at the tip of a soft finger to generate suction force and a selective sucking mode [5], [16]. Vacuum adhesion fails on porous or uneven surfaces. In contrast, dry adhesion, inspired by hierarchical micro/nanoscale fibrillary structures of gecko feet, forms van der Waals, requiring no energy supply and being relatively insensitive to surface materials. Various dry adhesives have been implemented in soft grippers. For instance, Sukho Song et al. proposed a gripper with mushroom-shaped adhesives capable of transfer-printing 3D parts [17]. However, these adhesives are complex to fabricate and difficult to detach as isotropic structure.

Received 23 January 2025; accepted 2 July 2025. Date of publication 11 July 2025; date of current version 21 July 2025. This article was recommended for publication by Associate Editor D. Aukes and Editor Y.-L. Park upon evaluation of the reviewers' comments. This work was supported by the National Natural Science Foundation of China under Grant 52375003 and Grant T2121003. *(Corresponding author: Kun Xu.)*

The authors are with the Robotics Institute of School of Mechanical Engineering and Automation, Beihang University (BUAA), Beijing 100191, China (e-mail: xk007@buaa.edu.cn).

This article has supplementary downloadable material available at https://doi.org/10.1109/LRA.2025.3588391, provided by the authors.

Digital Object Identifier 10.1109/LRA.2025.3588391

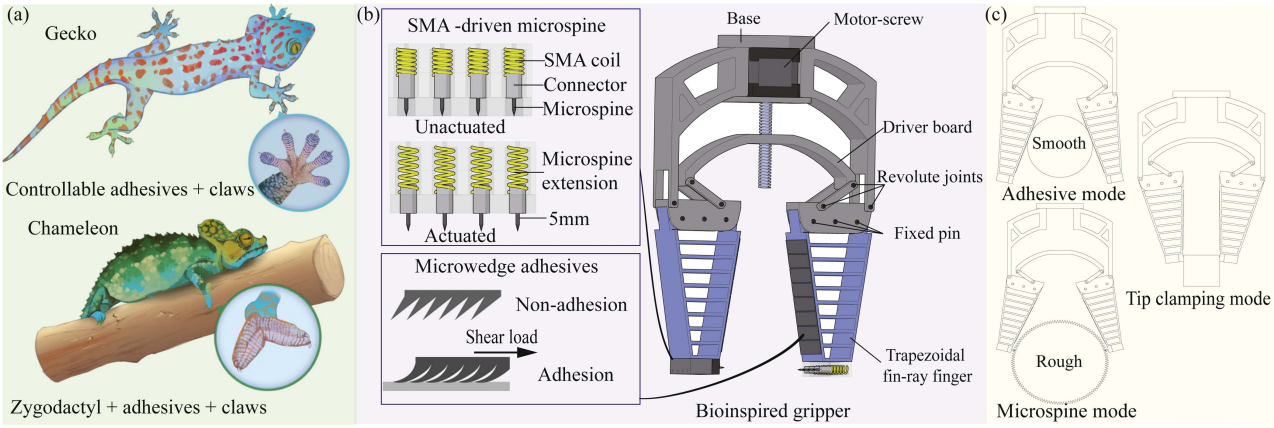

Fig. 1. Bioinspired soft gripper design. (a) Hybrid structures of microspines/claws and adhesives in gecko [26] and chameleon [27]. (b) Gripper design integrating microwedge adhesives and SMA-driven microspines. (c) Three operational modes: adhesive mode, microspine mode, and tip-clamping mode.

Microwedge adhesives, offering better control over engagement and disengagement, more closely mimic gecko feet properties. Mark R. Cutkosky et al. developed a series of shear-activated thin film soft grippers with microwedge adhesives. These grippers are compliant and capable of handling soft, brittle, fragile, or heavy objects with a light touch [18], [19]. However, despite dry-adhesion-based grippers having significantly enhanced grasping performance on smooth surfaces, they are ineffective on rough surfaces. To address this limitation, researchers incorporated microspine structures for rough surface adhesion. Examples include climbing robots such as Spinybot [20], RiSE [21], and LEMUR [22], [23], which can scale rough surfaces like brick walls, stucco, and outdoor rocks. Recently, Zi et al. [24] developed a spiny gripper inspired by beetle claws, featuring four bioinspired branches for achieve adaptive adhesion and detachment on rough surfaces. Similarly, Chen et al. [25] developed the ReachBot robot for planetary exploration, equipping it with a spiny gripper at the end of its extendable booms. However, these spinny grippers are primarily suited for rough surfaces, limiting their adaptability to other surface types.

In nature, lizard-like animals such as geckos and chameleons exhibit exceptional climbing abilities and wide movement range. Their feet combine micro/nanoscale fibrillary structures, effective on smooth surfaces, with claw-like structures at the toe tips for hooking onto rough surfaces such as rocks or tree bark, ensuring stable attachment [26], [27]. Inspired by hybrid adhesion mechanisms, soft grippers can effectively interact with unstructured environments. Despite this potential, few studies have truly integrated these mechanisms into a single device capable of switching seamlessly between different environments. Hu et al. developed a soft gripper that integrates flat dry adhesives, soft actuators, and microspines, enabling adaptable adhesion on both rough and smooth surfaces [28]. However, the flat dry adhesives lack controllability for attachment and detachment.

This study presents a dual-adhesion-enhanced soft gripper that integrates microwedge dry adhesives and SMA-driven (shape memory alloy) microspines. Inspired by the hybrid adhesion mechanisms of geckos and chameleons, the gripper achieves effective grasping and adhesion across object surfaces with varying roughness. Microwedge adhesives, inspired by the micro/nanofiber structures of gecko feet, enable controllable attachment and detachment on smooth surfaces. The SMA-driven microspines, functioning as a claw mechanism, are designed for rough surfaces and actively extend or retract depending on the environment, enabling transitions between adhesive, microspine, and tip-clamping modes. The gripper can envelop small objects while adhering to large-diameter surfaces. Both the dry adhesion and microspine components are insensitive to surface materials, enhancing the adaptability of the gripper to unpredictable environments.

II. Design, Analysis, and Optimization

A. Bioinspired Design of Soft Gripper

To adapt to complex natural environments, many animals have evolved hybrid adhesion mechanisms combining adhesives and claws. As shown in Fig. 1(a), gecko feet feature micro/nanoscale fibrillary adhesives and claws, enabling adaptation to both smooth and rough surfaces. Interestingly, the adhesives and claws exhibit similar attachment mechanics: adhesion occurs through shear loading, while detachment involves toe extension and eversion movements. Chameleons similarly employ zygodactyl structure integrating adhesives and claws to enhance grasping. Inspired by these hybrid adhesion mechanisms, a dual-adhesion-enhanced bioinspired soft gripper is proposed, combining microwedge dry adhesives with SMA-driven microspines, as illustrated in Fig. 1(b).

This two-finger structure incorporates trapezoidal fin-ray structures, featuring microspines modules on the top surface and internally positioned microwedge adhesives. This design mimics zygodactyl configuration of chameleons. The trapezoidal fin-ray fingers, with full passive adaptability and non-embedded actuation, provide exceptional surface adaptation.

The microwedge adhesives exhibit controllability similar to gecko feet. In the absence of shear load, only the tip of the microwedge contacts the surface, resulting in negligible adhesion. When a preferred shear load is applied, the microwedge structure bends, enabling adhesion. Upon release of

the shear load or when applied in a non-preferred direction, the adhesive detaches, mimicking the eversion motion of gecko feet.

The proposed SMA-driven microspine module consists of an SMA coil and a microspine in a single structure. The SMA coil, with its two-way shape memory effect, enables the microspine to extend and retract. The microspine, a sharp-tipped steel needle with a 0.8-mm diameter is arranged in four sets per finger, as shown in Fig. 1(b). Top-mounted microspines reduce interference with finger bending, unlike previous designs with SMA actuators on the finger back [28]. Specifically, without power, the microspine remains fully retracted within base. Conversely, when energized, the SMA coil extends, causing the microspine to protrude by 5 mm, facilitating grasping and manipulation of rough surfaces.

The proposed bioinspired soft gripper operates in three modes: adhesive, microspine, and tip clamping, as shown in Fig. 1(c). The adhesive mode is designed for smooth surfaces, with the microspines retracted to avoid damaging objects. A motor-driven vertical displacement of the driver board controls finger opening and closing, adjusting the grasping angle. Initially, only the microwedges tips contact the surface, resulting in minimal adhesion. As the fingers close, shear loading from the fin-ray crossbeam induces microwedge bending, increasing contact area and enhancing van der Waals forces. This enables stable attachment to large-diameter objects, which is challenging for non-adhesive grippers. Detachment is achieved by outward finger motion, emulating gecko toe eversion. In microspine mode, energizing the SMA coil causes it to elongate, extending the microspines, which penetrate rough or porous surfaces to create mechanical interlocking. For detachment, the SMA coil is de-energized, and the gripper opens outward, facilitating the release. In tip clamping mode, the SMA coil remains retracted, and the rigid outer frame facilitates grasping thin or small rigid objects, enabling precise manipulation.

B. Maximum Graspable Radius Analysis

Grasping radius and force are critical metrics for evaluating gripper performance. We simplified the nonlinear behavior of the finger during grasping and considered only the force interactions at the contact point between the finger and the object, as shown in Fig. 2(a). To determine the maximum graspable radius, let OE signify the screw, ED represent the driver board, OA and AB denote the bases, and $BGJK$ characterize the trapezoidal finger structure. The vertical motion of the driver board ED results in varying opening angles of the trapezoidal fingers, allowing the gripper to grasp objects of different sizes. A Cartesian coordinate system is established with O as the origin, where OA and OE represent the x axis and y axis, respectively. By solving the coordinates and corresponding angles of points A, B, C, D, E, G, J, H, and I, the geometric relationship between the gripper dimensions and the graspable radius can be determined.

The coordinates of points A, B, D and E are defined as A (l_{OA}, 0), B (l_{OA}, l_{AB}), D (l_{ED}, l_{OE}) and E (0, l_{OE}), where l_{OE} changes with the movement of the driver board. Given the coordinates and link lengths, we calculate the coordinates of point C, denoted as (x_c, y_c). Points B, C, and D form rotating

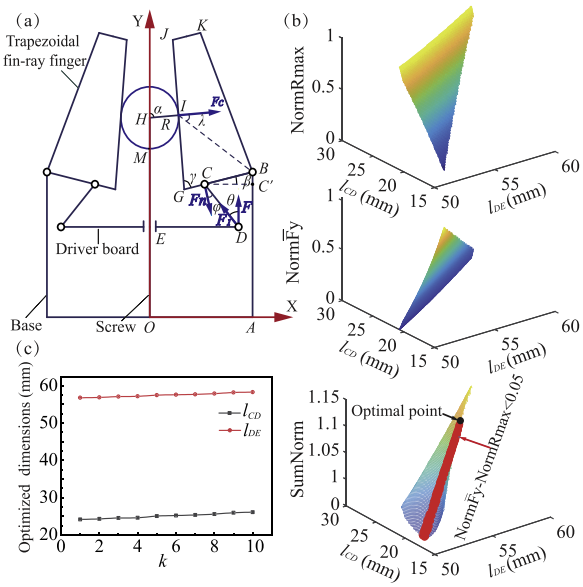

Fig. 2. Grasping optimization model. (a) Geometric relationships in the model. (b) Optimization results. (c) Results of sensitivity analysis.

pairs, with link BC rotating around point B and link CD rotating around point D. Point C represents the intersection of these two circular paths, yielding the following equations:

$$\begin{cases} (x_C - x_B)^2 + (y_C - y_B)^2 = {l_{BC}}^2 \\ (x_C - x_D)^2 + (y_C - y_D)^2 = {l_{CD}}^2 \end{cases} \tag{1}$$

Based on the geometric relationship, point C is always the upper intersection and its coordinates can be determined accordingly:

$$\begin{bmatrix} x_C \\ y_C \end{bmatrix} = \begin{bmatrix} p_1 y_C + p_2 \\ (-q_2 + \sqrt{q_2^2 - 4q_1 q_3})2q_1 \end{bmatrix} \tag{2}$$

where

$$\begin{cases} p_1 = -\dfrac{y_D - y_B}{x_D - x_B} \\ p_2 = \dfrac{l_{BC}^2 - l_{CD}^2 + x_D^2 - x_B^2 + y_D^2 - y_B^2}{2(x_D - x_B)} \\ q_1 = p_1^2 + 1 \\ q_2 = 2p_1(p_2 - x_B) - 2y_B \\ q_3 = (p_2 - x_B)^2 + y_B^2 - l_{BC}^2 \end{cases} \tag{3}$$

Point C, located on link BG, enables the determination of the coordinates of point G as follows:

$$\begin{bmatrix} x_G \\ y_G \end{bmatrix} = \begin{bmatrix} (l_{BG}x_C - l_{CG}x_B)/l_{BC} \\ (l_{BG}y_C - l_{CG}y_B)/l_{BC} \end{bmatrix} \tag{4}$$

Angle β, representing the angular position of link BC relative to the abscissa, can be calculated as:

$$\beta = \arccos\left((x_B - x_C)/l_{BC}\right) \tag{5}$$

where θ is the angle between vectors $\boldsymbol{P}_{DC}$ and the positive y-axis, with $\hat{\boldsymbol{y}} = [0, 1]^T$.

$$\theta = \arccos\left((y_C - y_D)/l_{CD}\right) \tag{6}$$

IEEE Robotics and Automation Letters (RA-L) paper, presented at ICRA 2026, Vienna, Austria. Cite as RA-L paper.

TABLE I
DESIGN PARAMETERS OF THE BASE, LINKS, AND FINGERS

Structure	Parameter	Structure	Parameter
Base l_{OA}	70 mm	Base thickness	35 mm
Base l_{AB}	100 mm	Finger height/thickness	100 /40 mm
Link l_{BC}	32.5 mm	Finger bottom l_{BG}	50 mm
Link l_{CD}	24.3 mm	Finger top l_{JK}	20 mm
Link l_{DE}	56.9 mm	Crossbeam thickness	2 mm
Gripper mass	539 g	Crossbeam number	8

For the isosceles trapezoidal finger structure, the l_{JG} is:

$$l_{JG} = \sqrt{((l_{BG} - l_{JK})/2)^2 + s^2} \tag{7}$$

where s is the vertical distance from JK to GB, representing the height of the finger. The coordinates of point J are then:

$$\begin{bmatrix} x_J \\ y_J \end{bmatrix} = \begin{bmatrix} x_G - l_{JG}\cos(\pi - \gamma - \beta) \\ y_G - l_{JG}\sin(\pi - \gamma - \beta) \end{bmatrix} \tag{8}$$

where γ is the base angle of the trapezoid, defined as $\gamma = \arctan(2s/(l_{BG} - l_{KJ}))$.

Assuming the grasped object is a cylinder, with its cross-sectional circle touching line segment JG on the inner side of the trapezoidal finger, and the center H $(0, h + R)$ directly above point O, the coordinates of the tangent point I :

$$\begin{bmatrix} x_I \\ y_I \end{bmatrix} = \frac{\boldsymbol{P}_{GJ}\boldsymbol{P}_{GJ}^T\boldsymbol{P}_{GH}}{\boldsymbol{P}_{GJ}^T\boldsymbol{P}_{GJ}} + \begin{bmatrix} x_G \\ y_G \end{bmatrix} \tag{9}$$

where $\boldsymbol{P}_{GJ}$ is a column vector.

The radius R of the grasped object is the vertical distance from the center H to side JG, and is represented as:

$$R = \frac{|Z_2(h + R) + Z_3|}{\sqrt{{Z_1}^2 + {Z_2}^2}} \tag{10}$$

where $Z_1 = y_J - y_G$, $Z_2 = x_G - x_J$, and $Z_3 = y_G x_J - y_J x_G$.

As the driver board moves, l_{OE} varies, yielding a series of R values. By comparison, the maximum value, $R_{\max}$, is then identified. Each pair of l_{CD} and l_{DE} determines a corresponding $R_{\max}$. To evaluate grasping performance in terms of both force and radius, the radius is normalized as:

$$\mathrm{Norm}R_{\max}(l_{CD}, l_{DE}) = \frac{R_{\max}(l_{CD}, l_{DE}) - \min R_{\max}}{\max R_{\max} - \min R_{\max}} \tag{11}$$

where $\max R_{\max}$ and $\min R_{\max}$ represent the maximum and minimum values from the series of $R_{\max}$, respectively.

Using the relationship between link CD, link DE, and radius derived from (11) and the data in Table I, the results are shown in the upper panel of Fig. 2(b). The effective range of l_{DE} is $[49.6,\ 59.6]$ mm, and that of l_{CD} is $[20.4,\ 27.75]$ mm. The figure indicates that the link DE has a greater impact on the grasping radius. Due to the coupled relationship between grasping force and radius, the two cannot reach their maximum values simultaneously. Therefore, further analysis of the grasping force is required.

C. Grasping Force Analysis

By analyzing the forces on each link, based on the motor input force and considering the torque balance at point B, a relationship between the grasping force and the gripper dimensions can be established. Assuming the motor applies a downward force F on the driver board, the force at point D is $F_1 = F/\cos\theta$. At point C, the force perpendicular to link BC is $F_n = F_1\cos\varphi$. Hence, the torque applied by the driving force F at point B is:

$$T_{iB} = F_n \cdot l_{BC} = F \cdot \cos\varphi \cdot l_{BC}/\cos\theta \tag{12}$$

Assuming the force acting upon the finger is F_c and originates from the grasped object, the torque produced by the finger at point B is:

$$T_{oB} = F_c \cdot l_{IB} \cdot \sin\lambda \tag{13}$$

Therefore, based on the torque balance at point B ($T_{iB} = T_{oB}$), the relationship between the grasping force F_c, the input force F, and the gripper dimensions can be derived as:

$$Fc = \frac{F \cdot \cos\varphi \cdot l_{BC}}{\cos\theta \cdot l_{IB} \cdot \sin\lambda} \tag{14}$$

In this context, F_c represents the grasping force, φ is the angle between F_1 and F_n, l_{IB} denotes the distance from tangent point I to point B, and λ is the angle between F_c and IB. To obtain the grasping force F_c, the angles φ, λ and link length l_{IB} must also be solved. Based on the perpendicular relationship between link BC and F_n, the coordinates of F_n can be determined, allowing the calculation of angle φ:

$$\varphi = \arccos\frac{(y_B - y_C)(x_D - x_C) + (x_C - x_B)(y_D - y_C)}{l_{BC}l_{CD}} \tag{15}$$

The angle λ between F_c and vector $\boldsymbol{P}_{IB}$ is:

$$\lambda = \arccos\left(\frac{\boldsymbol{P}_{F_c} \cdot \boldsymbol{P}_{IB}}{||\boldsymbol{P}_{F_c}|| \cdot ||\boldsymbol{P}_{IB}||}\right) \tag{16}$$

In this study, the vertical grasping force (F_y) is considered a key metric for evaluating grasping performance. Based on the previously determined F_c, F_y can be calculated as:

$$F_y = F_c(\cos\alpha + \mu\sin\alpha) \tag{17}$$

where μ is the friction coefficient, and α represents the angle between F_c and the positive y-axis.

According to (17), the vertical grasping force (F_y) consists of two components. When $\alpha < \pi/2$, $F_c\cos\alpha$ acts in the negative y-direction, contributing to the envelopment of the object. Conversely, when $\alpha > \pi/2$, $F_c\cos\alpha$ acts in the positive y-direction, reducing the vertical grasping force F_y. For each set of defined lengths l_{CD}, l_{DE}, and l_{OE}, a corresponding F_y is determined. To ensure the gripper maintains sufficient grasping force at every position as l_{OE} varies, the average value of F_y is calculated.

$$\bar{F}_y = \frac{\int_{l_{OE\min}}^{l_{OE\max}} F_y(l_{CD}, l_{DE})}{l_{OE\max} - l_{OE\min}} \tag{18}$$

Using the same method as (11), the normalized $\mathrm{Norm}\bar{F}_y$ was calculated, as shown in the middle panel of Fig. 2(b). Based on the simulation results, the relationship between link lengths and

IEEE Robotics and Automation Letters (RA-L) paper, presented at ICRA 2026, Vienna, Austria. Cite as RA-L paper.

grasping force is determined. The effective range of the links is consistent with the radius calculation. However, unlike the radius, link CD has a greater impact on force.

D. Optimization and Analysis of Link Dimensions

Based on the relationships between grasping radius, grasping force, and gripper dimensions, we need to optimize the link dimensions to achieve excellent performance. When l_{OA} and l_{AB} are undefined, the gripper size can theoretically become infinite, leading to indeterminate values for both the maximum grasping radius and maximum grasping force. Therefore, with l_{OA}, l_{AB}, and l_{BC} fixed, the optimal link lengths l_{DE} and l_{CD} are determined by maximizing both grasping radius and grasping force. The objective function is defined as:

$$\mathrm{Max}FR(l_{CD}, l_{DE}) = \mathrm{Norm}\bar{F}_y + \mathrm{Norm}R_{\max} \tag{19}$$

In this function, Norm denotes value normalization within maximum and minimum thresholds. The first term represents the average vertical grasping force achievable by the gripper during the motion of the driver board. The average grasping force is calculated to ensure balanced grasping performance across the entire range of l_{OE} variations, rather than optimizing for a single position. The second term represents the maximum graspable radius, and $l_{OE\min}$ and $l_{OE\max}$ denote the range of motion for the driver board. Under the real-world application scenarios, the following constraints are proposed.

In (19), one component may be disproportionately large. To ensure balanced performance and give equal weight to both terms, the following constraint is applied:

$$\left|\mathrm{Norm}\bar{F}_y - \mathrm{Norm}R_{\max}\right| < 0.05 \tag{20}$$

The motor is fixed at point O with a constant height of 32.5 mm, setting $l_{OE\min} = 32.5$ mm. When the inner surface JG of the finger exceeds the vertical position, it can no longer support objects, reducing graspable payload. The maximum l_{OE} occurs when JG is perpendicular to the x-axis, as defined by the vertical constraint:

$$l_{OE\max} = l_{AB} - l_{BC}\sin\beta - \sqrt{l_{CD}^2 - (l_{DE} - l_{OA} + l_{BC}\cos\beta)^2} \tag{21}$$

where $\beta = \pi/2 - \gamma$.

To ensure a rational design of the links, the following constraint is proposed:

$$l_{BC} + l_{CD} > l_{BD} \tag{22}$$

Using the dynamic grasping optimization model, the grasping optimization algorithm is summarized as follows:

The actual design parameters of the gripper, listed in Table I, are used as inputs for the optimization model. The output results are obtained as shown in the bottom panel of Fig. 2(b). The red region indicates the weight constraints. At a friction coefficient of 0.2, the optimized link lengths $l_{CD} = 24.3$ mm, $l_{DE} = 56.9$ mm can be determined. Under variations in finger stiffness, the friction coefficient in the model also changes. We introduce an equivalent friction coefficient defined as $\mu = 0.1k$, where $k = \{1, \ldots, 10\}$. Different values of k represent different finger materials or stiffness. Based on the proposed optimization model, the relationship between k and the optimized linkage dimensions is illustrated in Fig. 2(c). The results indicate that the optimal link dimensions exhibit limited sensitivity to changes in friction, suggesting the robustness of the proposed optimization strategy.

Algorithm 1: Grasping Optimization Algorithm.

Input: input parameters l_{OA}, l_{AB}, l_{BC}, l_{BG}, s, γ, μ, F.
Discretizing l_{CD} yields $l_{CD}(i)$, $i = 1, 2, ..., N_i$;
Discretizing l_{DE} yields $l_{DE}(j)$, $j = 1, 2, ..., N_j$;
for *each* $l_{CD}(i)$ **do**
  for *each* $l_{DE}(j)$ **do**
    calculate $l_{OE\max}$ by Eq. (21)
    Discretizing $l_{OE} \in [l_{OE\min}, l_{OE\max}]$ yields $l_{OE}(k)$, $k = 1, 2, .., N_k$
    for *each* $l_{OE}(k)$ **do**
      calculate coordinates of points C, G, I, J;
      calculate angle $\beta(i,j,k), \theta(i,j,k), \varphi(i,j,k)$;
      calculate radius $R(i,j,k)$; calculate $F_y(i,j,k)$.
    end
    Search maximum $R_{\max}(i,j)$ **in** $R(i,j,k)$;
    $FR(i,j)$ = Norm$\bar{F}_y(i,j)$ + Norm$R_{\max}(i,j)$;
  end
end
Search maximum FR and its $i_{\max}$, $j_{\max}$ **in** $FR(i,j)$
Output: $i_{\max}$, $j_{\max}$
Return l_{CD}, l_{DE}

III. Experiments and Results

A. Prototype Fabrication

The gripper base and links were 3D printed. The actuator comprises a 35 × 32 mm stepper motor with a thrust capacity of 130 N, coupled with an 8-mm diameter lead screw with a 2-mm pitch (Chongqing UMot Technology Co., Ltd). The trapezoidal fin-ray fingers were fabricated via silicone vacuum molding using a Shore A80 elastomer. The proposed gripper weighs 539 g with the motor and 318 g without. The design parameters of the base, links, and fingers are listed in Table I.

The microwedge adhesive was prepared by casting elastomer material (Sylgard 170, Dow Corning) into a microwedge mold, created by making cuts in wax using a sharp, lubricated tool (Leica 819, Low Profile, Microtome Blades). This process formed negative cavities of a microwedge shape, followed by post-treatment with chemical vapor deposition [29], as shown in Fig. 3(a). Each microwedge measures approximately 105 μm in height, 75 μ m in width and inclined at 45°. The microwedge adhesive unit (9 mm wide, 40 mm long) were aligned along the gripper crossbeam and bonded to the inner side of the fingers. Eight adhesive patches were mounted on each finger with defined spacing.

The microspine structure comprises an SMA coil and a 3D printed cylinder with an interference fit inside the SMA coil. A needle, 0.8 mm in diameter with a sharp tip, was inserted into a

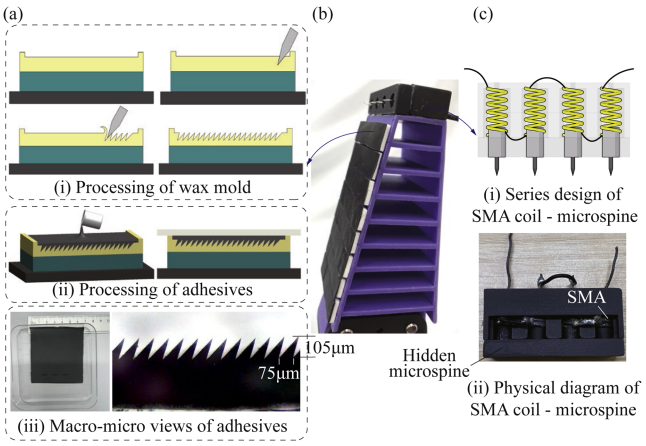

Fig. 3. Fabrication process of the soft gripper. (a) Fabrication of microwedge adhesives. (b) Finger integrating microwedge adhesives and microspines. (c) Design and physical diagram of the SMA coil-microspine structure.

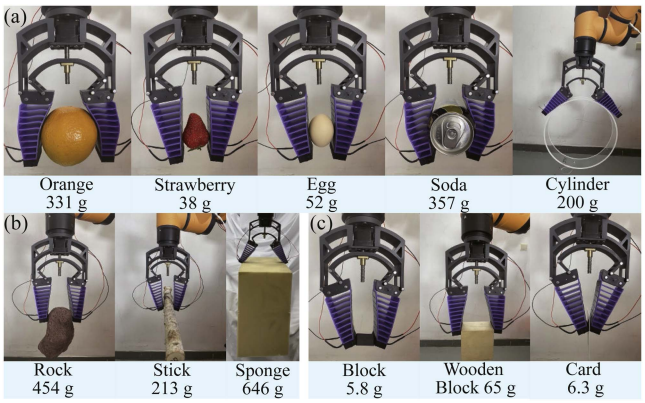

Fig. 4. Grasping performance with various objects. (a) Adhesive mode. (b) Microspine mode. (c) Tip clamping mode.

hole in the cylinder, protruding by 5 mm. The SMA coil has an internal diameter of 4.2 mm, an external diameter of 5.8 mm, a wire diameter of 0.8 mm, and an original length of 10 mm. When heated, it extends by more than 15 mm. The SMA coil is aligned coaxially in a base hole, with its lower end straightened and secured with glue for stability. Four microspine structures were mounted on each finger, with the SMAs connected in series for synchronized extension, requiring only two input/output wires, as shown in Fig. 3(c).

B. Grasping Performance With Different Objects

We conducted experiments to evaluate the grasping and adhesion performance of the gripper on irregularly shaped objects with varied surface textures. Mounted on the end of a robotic arm (UR5, Universal Robots), the gripper performed grasping, lifting, holding, and releasing tasks. In adhesive mode, the gripper successfully grasped delicate objects such as oranges, strawberries, eggs, soda bottles, and a 260-mm diameter smooth acrylic cylinder, as shown in Fig. 4(a). This mode not only enabled the handling of fragile objects but also demonstrated effective adhesion to large-diameter surfaces. In microspine

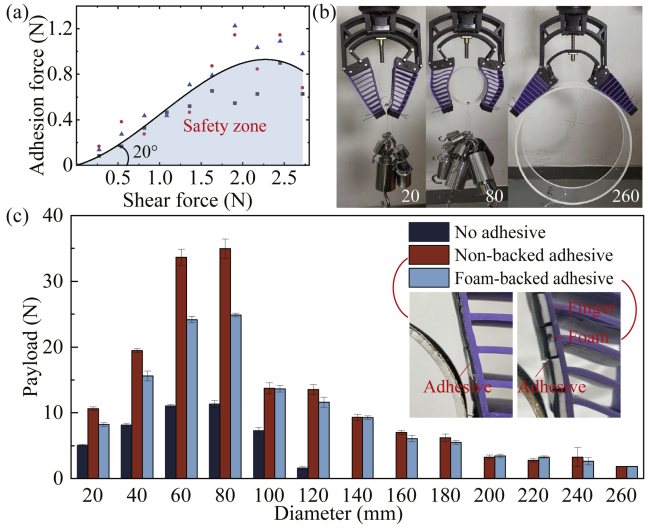

Fig. 5. Test results on smooth surfaces. (a) Normalized shear and normal adhesion forces. (b) Gripper with non-backed adhesives grasping 20, 80, and 260 mm objects. (c) Performance comparison of grippers without adhesives, with non-backed adhesives, and with foam-backed adhesives.

mode, the gripper grasped porous rocks, a rough tree trunk (3 cm in diameter and 40 cm in length), and a sponge (35 × 35 × 20 cm) by extending microspines that penetrated rough surfaces and hooked onto protrusions, ensuring stable grasping, as shown in Fig. 4(b). Finally, in tip clamping mode, the rigid outer frame of the SMA-driven microspines enabled grasping of small objects and thin cards, as shown in Fig. 4(c).

C. Grasping Performance on Smooth Surfaces

A single adhesive unit was tested using a 6-axis force/torque sensor. As shown in Fig. 5(a), the measured shear and normal adhesion forces per square centimeter reached maximum values of 2.72 and 1.14 N, respectively. Stable attachment was achieved when the applied load angle was less than 20°, corresponding to the blue region in the figure. Furthermore, the gripper was used to grasp acrylic cylinders with varying diameters to evaluate adhesion performance on smooth surfaces, as shown in Fig. 5(b). The dynamic grasping procedure from the above tests was applied to determine the maximum grasping payload for each diameter, with three repetitions. Grippers with foam-backed adhesives, non-backed adhesives, and without adhesives were tested. The results are shown in Fig. 5(c).

The results revealed several key findings. First, regardless of adhesive type, grasping payload initially increased and then decreased with diameter. For smaller diameters, reduced contact area led to lower friction, while for larger diameters, the shift in grasping force direction (from top to bottom) resulted in reduced payload. Here, the large diameter refers to the distance beyond the inner side of the finger when it is parallel. Larger diameters also reduced the loading distance and adhesive contact area at the proximal end of the finger. Then, grippers equipped with adhesives clearly outperform those without. Specifically, grippers with non-backed adhesives achieved a maximum grasping payload of 34.9 N and a maximum grasping diameter of 260 mm,

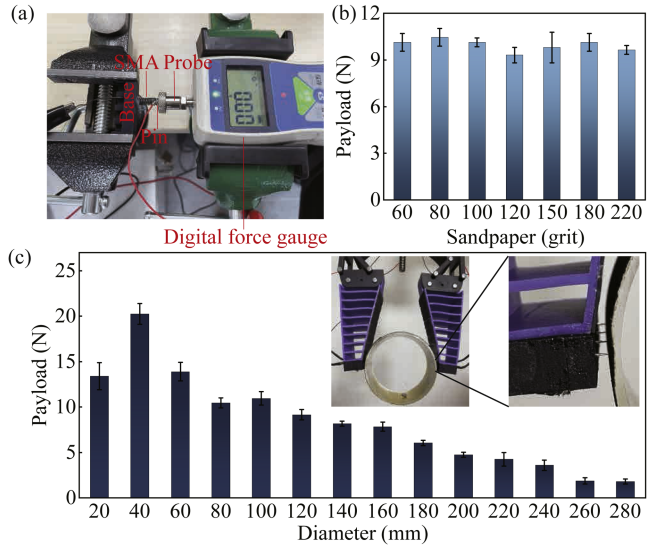

Fig. 6. Test results on rough surfaces. (a) Force measurement setup for a single SMA actuator. (b) Relationship between sandpaper roughness and payload. (c) Impact of object diameter on payload for rough surfaces.

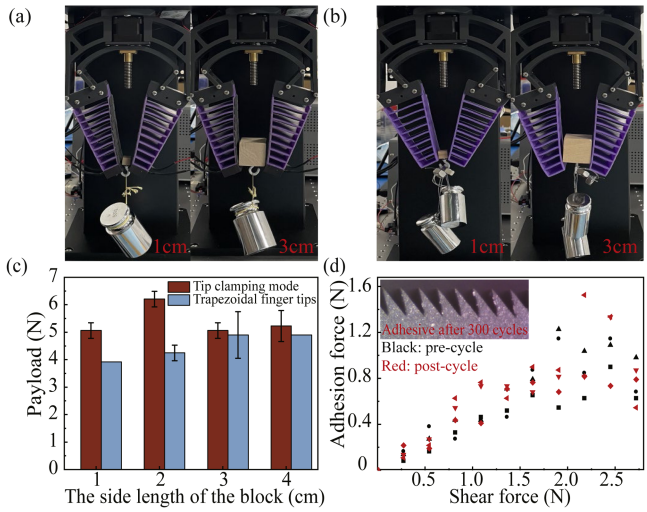

Fig. 7. Grasping Evaluation. (a) Tip-clamping grasp of 1-cm and 3-cm wooden blocks. (b) Grasping the same blocks using a trapezoidal fingertip. (c) Comparison of maximum payloads for both methods. (d) Adhesion force of the microwedge adhesive before and after 300 grasp-release cycles.

compared with 11.3 N and 120 mm for those without adhesives, representing 209% and 117% improvements. For diameters below 100 mm, grippers with non-backed adhesives outperformed those with foam-backed adhesives. However, for larger diameters, both types exhibited similar grasping performance, suggesting that foam-backed adhesives influence the bending deformation at smaller diameters ($<$ 100 mm).

D. Grasping Performance on Rough Surfaces

The performance of a single SMA coil–microspine unit was evaluated under input voltages of 1.0, 1.2, and 1.4 V (three trials each). Higher voltages reduced the extension time (from 33.0 to 16.7 s) but increased the retraction time due to heat buildup (from 80.3 to 90.6 s). The output force remained stable ($\approx$ 5.1N), as measured using the experimental setup shown in Fig. 6(a), indicating that voltage primarily affects actuation speed rather than force. Based on the single-SMA results, a 2.5 V, 1.5 A input was applied to the four-SMA series configuration, yielding extension and retraction times of 33 and 80 s, respectively. For rough surface testing, the gripper was tested on acrylic cylinders with varying diameters covered with 60-grit sandpaper, as well as cylinders with an 80-mm diameter covered in sandpaper of varying roughness. The extended microspines interacted with the rough surface, preventing adhesive damage, as shown in Fig. 6(c). Comparing the results Fig. 6(b) with Fig. 6(c), it is evident that the diameter of the grasped object has a more significant influence on the grasping payload than the surface roughness. As the sandpaper roughness increased from 60 to 220 grit, the change in the gripped weight was minimal. This indicates the insensitivity of the gripper to existing surface roughness variations, with more substantial roughness increases needed to significantly affect grasping performance.

Test results on rough cylinders with varying diameters (Fig. 6(c)) show that the maximum payload of 20.3 N in the microspine mode with a 40-mm diameter. For 20-mm-diameter cylinders, the small diameter cause instability, resulting in a reduced payload. As the diameter exceeded 40 mm, the payload decreased due to the varying bending states of the fingertips and varying insertion angles of the microspines. With larger diameters, the microspines becomes more vertical, diminishing grasping performance.

E. Grasping Performance Under Tip Clamping Mode

To evaluate the grasping performance under the tip clamping mode, we employed the rigid outer frame at the fingertip to grasp wooden blocks with edge lengths ranging from 1 cm to 4 cm, and measured the corresponding maximum payload, as shown in Fig. 7(a). Furthermore, we conducted the same set of experiments using trapezoidal fingertip structures, as shown in Fig. 7(b), and the results of both configurations were compared, as summarized in Fig. 7(c). In tip clamping mode, the maximum payload reached 6.2 N when grasping a 2-cm block. The higher rigidity of the outer frame increases the grasping force, thereby enhancing stability during the manipulation of small objects and facilitating more precise operations. Moreover, it prevents direct contact between the object and adhesives.

IV. Discussiom

A comparative analysis with state-of-the-art soft grippers was conducted, focusing on actuation, adhesion enhancement strategy, payload, and surface adaptability, as summarized in Table II. The proposed gripper demonstrates superior surface adaptability and competitive payload capacity for both smooth and rough surfaces. While performance is slightly lower than grippers specialized for single-surface operation, this is attributed to the non-embedded actuation and limited microspine count (four per finger). Future work will explore stiffness–adaptability tradeoffs and increase microspine density to enhance performance.

TABLE II
COMPARISON WITH STATE-OF-THE-ART GRIPPERS

Ref.	Actuation	Enhanced strategy	Payload (N)	Adaptability
[14]	P	Adhesive	>19.6	S
[13]	P	Adhesive	28.29	S
[5]	T&P	Vacuum	>40	S
[25]	T	Microspine	>34.2	R
[24]	Link&T	Microspine	39.7/47.5	R
[15]	T	Adhesive&Electrostatic	>13	S
[28]	SMA	Adhesive&Microspine	8.9(S)/3.5(R)	S&R
Ours	Link&SMA	Adhesive&Microspine	34.9(S)/20.4(R)	S&R

Note: S-smooth, R-rough, P-Pneumatics, T-Tendon. Fingertips in [5] and [13] are limited to smooth surfaces. In [24], the normal and shear payloads reached 39.7 and 47.5 N, respectively.

SMA coil actuators exhibit lifespans of tens of thousands of cycles, contributing minimally to overall gripper wear. To evaluate the durability of the microwedge adhesive, 300 grasp-release cycles were performed by grasping an 80-mm diameter acrylic cylinder with a 3-kg payload. Adhesion was measured before and after cycling, as shown in Fig. 7(d), using a test unit taken from the midsection of the finger, where the load is most concentrated. Black and red data represent pre- and post-cycle adhesion, respectively, indicating minimal degradation. Microscopy after cycling confirms intact microwedge structures, with only minor surface contamination removable by alcohol cleaning.

V. CONCLUSION AND OUTLOOK

The bioinspired soft gripper proposed in this paper is enhanced by microwedge adhesives and SMA-driven microspines, demonstrating excellent grasping and adhesion performance on both rough and smooth surfaces with varying curvature. The grasping optimization model elucidates the relationships among grasping force, grasping radius, and gripper dimensions, allowing the identification of optimal link dimensions. Testing showed that the gripper with non-backed adhesives achieved the best grasping performance on smooth surfaces, with a maximum payload of 34.9 N and a maximum grasping diameter of 260 mm—209% and 117% increases compared with the gripper without adhesives. On rough surfaces, the microspine mode supported a maximum payload of 20.4 N and a grasping diameter of 280 mm. In tip clamping mode, the maximum payload reached 6.2 N when grasping a 2 cm block. Further work will focus on enhancing the grasping performance and integrating sensors into the soft fingers to autonomously select between microspine, adhesive, or tip clamping modes based on object roughness and size.

REFERENCES

[1] J. Langowski, P. Sharma, and A. L. Shoushtari, "In the soft grip of nature," *Sci. Robot.*, vol. 5, no. 49, 2020, Art. no. eabd9120.

[2] J. Shintake, V. Cacucciolo, D. Floreano, and H. Shea, "Soft robotic grippers," *Adv. Mater.*, vol. 30, no. 29, 2018, Art. no. 1707035.

[3] S. Liu, F. Wang, Z. Liu, W. Zhang, Y. Tian, and D. Zhang, "A two-finger soft-robotic gripper with enveloping and pinching grasping modes," *IEEE/ASME Trans. Mechatron.*, vol. 26, no. 1, pp. 146–155, Feb. 2021.

[4] S. Ku, B. -H. Song, T. Park, H. -Y. Kim, and Y. -L. Park, "Multifunctional soft gripper with microneedles and integrated sensing for robotic fabric handling," *IEEE/ASME Trans. Mechatron.*, vol. 29, no. 2, pp. 866–877, Apr. 2024.

[5] B. Fang et al., "Multimode grasping soft gripper achieved by layer jamming structure and tendon-driven mechanism," *Soft Robot.*, vol. 9, no. 2, pp. 233–249, 2022.

[6] W. Ruotolo, D. Brouwer, and M. R. Cutkosky, "From grasping to manipulation with gecko-inspired adhesives on a multifinger gripper," *Sci. Robot.*, vol. 6, no. 61, 2021, Art. no. eabi9773.

[7] I. A. Anderson, T. A. Gisby, T. G. McKay, B. M. O'Brien, and E. P. Calius, "Multi-functional dielectric elastomer artificial muscles for soft and smart machines," *J. Appl. Phys.*, vol. 112, no. 4, 2012, Art. no. 041101.

[8] W. Xu, H. Zhang, H. Yuan, and B. Liang, "A compliant adaptive gripper and its intrinsic force sensing method," *IEEE Trans. Robot.*, vol. 37, no. 5, pp. 1584–1603, Oct. 2021.

[9] X. Cai and B. Tang, "Mechanically controlled robotic gripper with bistability for fast and adaptive grasping," *Bioinspiration Biomimetics*, vol. 18, no. 1, 2022, Art. no. 014001.

[10] H. Li, P. Zhou, S. Zhang, J. Yao, and Y. Zhao, "A high-load bioinspired soft gripper with force booster fingers," *Mechanism Mach. Theory*, vol. 177, 2022, Art. no. 105048.

[11] W. Zhu et al., "A soft-rigid hybrid gripper with lateral compliance and dexterous in-hand manipulation," *IEEE/ASME Trans. Mechatron.*, vol. 28, no. 1, pp. 104–115, Feb. 2023.

[12] H. Jeong and J. Kim, "Ossicle reinforced porous structure for variable stiffness soft actuator inspired from echinoderms," *IEEE/ASME Trans. Mechatron.*, vol. 28, no. 6, pp. 3551–3561, Dec. 2023.

[13] W. Park, S. Park, H. An, M. Seong, J. Bae, and H. E. Jeong, "A sensorized soft robotic hand with adhesive fingertips for multimode grasping and manipulation," *Soft Robot.*, vol. 11, pp. 698–708, 2024.

[14] T. Sun et al., "A versatile and high-load soft gripper enabled by vacuum-assisted bio-inspired interfacial adhesion," *Smart Mater. Structures*, vol. 33, no. 1, 2024, Art. no. 015034.

[15] V. Alizadehyazdi, M. Bonthron, and M. Spenko, "An electrostatic/gecko-inspired adhesives soft robotic gripper," *IEEE Robot. Automat. Lett.*, vol. 5, no. 3, pp. 4679–4686, Jul. 2020.

[16] F. Liu, F. Sun, B. Fang, X. Li, S. Sun, and H. Liu, "Hybrid robotic grasping with a soft multimodal gripper and a deep multistage learning scheme," *IEEE Trans. Robot.*, vol. 39, no. 3, pp. 2379–2399, Jun. 2023.

[17] S. Song, D. -M. Drotlef, C. Majidi, and M. Sitti, "Controllable load sharing for soft adhesive interfaces on three-dimensional surfaces," *Proc. Nat. Acad. Sci.*, vol. 114, no. 22, pp. E4344–E4353, 2017.

[18] E. W. Hawkes, H. Jiang, D. L. Christensen, A. K. Han, and M. R. Cutkosky, "Grasping without squeezing: Design and modeling of shear-activated grippers," *IEEE Trans. Robot.*, vol. 34, no. 2, pp. 303–316, Apr. 2018.

[19] J. Hashizume, T. M. Huh, S. A. Suresh, and M. R. Cutkosky, "Capacitive sensing for a gripper with gecko-inspired adhesive film," *IEEE Robot. Automat. Lett.*, vol. 4, no. 2, pp. 677–683, Apr. 2019.

[20] A. T. Asbeck, S. Kim, M. R. Cutkosky, W. R. Provancher, and M. Lanzetta, "Scaling hard vertical surfaces with compliant microspine arrays," *Int. J. Robot. Res.*, vol. 25, no. 12, pp. 1165–1179, 2006.

[21] M. J. Spenko et al., "Biologically inspired climbing with a hexapedal robot," *J. field Robot.*, vol. 25, no. 4/5, pp. 223–242, 2008.

[22] A. Parness et al., "Gravity-independent rock-climbing robot and a sample acquisition tool with microspine grippers," *J. Field Robot.*, vol. 30, no. 6, pp. 897–915, 2013.

[23] A. Parness, N. Abcouwer, C. Fuller, N. Wiltsie, J. Nash, and B. Kennedy, "LEMUR 3: A limbed climbing robot for extreme terrain mobility in space," in *Proc. 2017 IEEE Int. Conf. Robot. Automat.*, 2017, pp. 5467–5473.

[24] P. Zi, K. Xu, Y. Tian, and X. Ding, "A mechanical adhesive gripper inspired by beetle claw for a rock climbing robot," *Mechanism Mach. Theory*, vol. 181, 2023, Art. no. 105168.

[25] T. G. Chen et al., "Locomotion as manipulation with reachbot," *Sci. Robot.*, vol. 9, no. 89, 2024, Art. no. eadi9762.

[26] A. P. Russell, "Descriptive and functional anatomy of the digital vascular system of the tokay, gekko gecko," *J. Morphol.*, vol. 169, no. 3, pp. 293–323, 1981.

[27] M. Spinner, G. Westhoff, and S. N. Gorb, "Subdigital setae of chameleon feet: Friction-enhancing microstructures for a wide range of substrate roughness," *Sci. Rep.*, vol. 4, no. 1, 2014, Art. no. 5481.

[28] Q. Hu, E. Dong, and D. Sun, "Soft gripper design based on the integration of flat dry adhesive, soft actuator, and microspine," *IEEE Trans. Robot.*, vol. 37, no. 4, pp. 1065–1080, Aug. 2021.

[29] Z. Chu, C. Wang, X. Hai, J. Deng, J. Cui, and L. Sun, "Analysis and measurement of adhesive behavior for gecko-inspired synthetic microwedge structure," *Adv. Mater. Interfaces*, vol. 6, no. 12, 2019, Art. no. 1900283.